High-fidelity conical piezoelectric transducers and finite element models utilized to quantify elastic waves generated from ball collisions

Gregory C. McLaskey[1], Steven D. Glaser
Department of Civil and Environmental Engineering, University of California, Berkeley, USA

ABSRACT

Experimental studies were performed using high-fidelity broadband Glaser-NIST conical transducers to quantify stress waves produced by the elastic collision of a tiny ball and a massive plate. These sensors are sensitive to surface-normal displacements down to picometers in amplitude, in a frequency range of 20 kHz to over 1 MHz. Both the collision and the resulting transient elastic waves are modeled with the finite element program ABAQUS and described theoretically through a marriage of the Hertz theory of contact and a full elastodynamic Green's function found using generalized ray theory. The calculated displacements were compared to those measured through the Glaser-NIST sensors.

Keywords: sensor calibration, impact, finite element analysis, acoustic emission, wave propagation

1. INTRODUCTION

For quantitative experimentation, the data is only as good as the sensor calibration. For an absolute calibration scheme to be effective, a known source must be employed and a model must be developed which maps this source to a disturbance which excites the sensor in a known and repeatable fashion. This source and model combination offers a baseline from which the sensor's output can be evaluated. For ultrasonic piezoelectric transducers, finding a source which can accommodate the range of frequencies and amplitudes over which the calibration is to be valid is not a trivial matter.

The sensor described in this paper is a high-fidelity conical piezoelectric transducer which is sensitive to surface-normal disturbances on the order of a picometer in amplitude, in the frequency range between 8 kHz and 2 MHz. For sensors of this type, a glass capillary fracture or the breaking of a mechanical pencil lead are common calibration sources[1,2]. A less common source is the impact of a ball on a massive body[2], and it is this source which is the topic of the present paper. The glass capillary and pencil lead sources are known to introduce a forcing function which is very nearly a step function in time, while the ball source is more impulsive in nature. The ball source is an intuitively simple source, and it delivers a finite impulse to the body[2]. Both of these characteristics lend themselves well to modeling, both analytically and numerically.

This paper describes experiments and models for a sensor calibration process using the collision of a sphere on a massive body as the forcing function. First, the theoretical developments of Hertz impact theory are reviewed. Next, the equations of motion which govern wave propagation in an elastic solid are discussed and solutions to the wave propagation problem are reviewed. In Section four, the finite element numerical model is described. Section five describes the experimental procedures used for the calibration. Finally, the results are presented and the limitations of the finite element models are addressed.

2. HERTZ THEORY OF ELASTIC IMPACT

Hertzian theory has been employed in the vast majority of theoretical work concerning the elastic collision of two bodies. (For a review of this work see Love[3], Johnson[4], or Goldsmith[5].) The Hertz theory of impact is formulated from the stress equilibrium equation and the force deformation relation:

$$f = k_1 \alpha^{3/2}, \tag{1}$$

[1] gmclaskey@berkeley.edu

where f is the force acting between the bodies, α is the approach, (a distance which represents the maximum relative compression between the two bodies), and k_1 is a constant which depends on the geometry and material properties of the two bodies. This quasistatic formulation completely ignores the existence of transient stress waves, yet despite this limitation, the results of Hertz's original calculations are extremely robust, and have been verified experimentally[4,5].

The force between a sphere and a massive body can be found from Newton's laws[3] as the rate of change in momentum:

$$f = m_1 \frac{d^2\alpha}{dt^2}, \tag{2}$$

where m_1 is the mass of the sphere. By equating Equations 1 and 2, the maximum compression α_{max}, which occurs at the instant of zero velocity, can be expressed as:

$$\alpha_{\max} = \left[\frac{15\pi v_0^{\,2}(\delta_1 + \delta_2) m_1}{16\sqrt{R_1}} \right]^{2/5}. \tag{3}$$

From this formulation, one can calculate the contact duration

$$t_c = 4.53\left(4\rho_1\pi(\delta_1 + \delta_2)/3\right)^{2/5} R_1 v_0^{\,-1/5} \tag{4}$$

and α as a function of time

$$\alpha(t) = \alpha_{\max}\phi(v_0 t/\alpha_{\max}), \tag{5}$$

where $\delta_i = \frac{1-\nu_i^{\,2}}{\pi E_i}$, (6)

and E, ρ, and ν are the Young's modulus, density, and poisson's ratio, respectively, and the origin at time t = 0 is the initiation of contact. Subscript 1 refers to the material of the sphere and subscript 2 refers to the material of the massive body (a thick plate in the present case). R_1 is the radius of the sphere, and v_0 is the incoming velocity of the sphere.

Hunter[6] found Equation (5) to be very well approximated by the function

$$\alpha(t)=\alpha_{max}\sin(\pi t/t_c) \qquad 0 \le |t| \le t_c \tag{7}$$

The force between the ball and plate can be found by plugging Equation 7 into Equation 1[4,5]

$$f(t) = f_{\max}\sin(\pi t/t_c)^{3/2} \qquad 0 \le |t| \le t_c, \tag{8}$$

where the maximum force is

$$f_{\max} = 1.917\rho_1^{\,3/5}\left(\delta_1 + \delta_1\right)^{-2/5} R_1^{\,2} v_0^{\,6/5}. \tag{9}$$

The two most relevant parameters for this study are the contact time t_c, and the maximum force between the two bodies f_{max}.

3. WAVE PROPAGATION

Historically, the first consideration of the stress waves produced by rapidly changing forces at the surface of an elastic half space was by Lamb[7]. Extension of the theory for specific geometries and loading situations has been completed by many researchers[8-10], and today displacements produced by forces acting on the surface of a material are well known[12,13].

The Elastodynamics off stresses and strains in an elastic medium are governed by Navier's equation, which can be derived[13] by substituting the appropriate definition for strain and the stress-strain relationship into the stress equations of motion:

$$\rho\frac{\partial^2 u_i}{\partial t^2} = f_i + (C_{ijkl}(u_{k,l} + u_{l,k})/2)_{,j} \tag{10}$$

where u_i is the displacement vector of a material point, C_{ijkl} is the fourth order elastic strain tensor, and f_i is a body force applied to the material. For the purpose of sensor calibration, we seek solutions in the form of a Green's function, $G_{in}(x,t;\xi,\tau)$, which describes the displacement at point x at time t due to a unit impulse at location ξ in the

direction n at time τ. The Green's function can be thought of as the impulse response function of an elastic material that maps the dynamic force field at location ξ to a mechanical disturbance u_i at the sensor site x. Under the definition of the Green's function, the displacement at the sensor location can be expressed as

$$u_i(x,t) = G_{in}(x,t;\xi_0,\tau) \otimes f_n(\xi_0,\tau), \tag{11}$$

where $\otimes$ represents convolution in time. In this formulation all forces are assumed to act at the point ξ_0 and $f_n(\xi_0, \tau)$ is the sum of these forces. In the case of a ball impact, the force is assumed to act solely in the direction normal to the surface of the massive plate and the displacement is measured solely in the direction normal to the surface of the plate. Under these conditions, Equation 11 reduces to the scalar equation:

$$u_3(t) = f_3(\xi_0,\tau) \otimes g_{33}(x_0,t;\xi_0,\tau). \tag{12}$$

By inversion, the force-time function $f_n(\tau)$ at the source location ξ_0 can be determined from the measured displacements and a known Green's function, and this can be compared to Hertz theory (Equation 8).

A number of strategies have been employed to solve for the Green's functions either analytically (typically with the use of Fourier and Laplace transforms) or numerically. Closed-form analytical solutions currently exist for the whole space[12,13], half space[9,13], and infinite plate[10,11]. For this work, a solution scheme known as the generalized ray theoretical solution[14] has been used for an infinite plate geometry[15]. This solution was checked against theoretical solutions[9,10].

4. NUMERICAL MODELS

Numerical schemes can be employed to solve Equation 10 for complicated geometries and boundary conditions. Relevant numerical solutions can be validated against analytical solutions found for simpler geometries. For this work, the commercial finite element software ABAQUS[16] was used to find the displacements which arise from rapidly changing point loads such as those described in Equation 8. Additionally, the whole Hertzian contact problem can be modeled with the finite element code. One such model is shown in Figure 1. The model consists of two elastic bodies (a 1.58 mm sphere and a massive 50 mm thick plate in this case) which are made to collide at a set initial velocity.

The finite element models used in this study are composed of three-node linear axisymmetric triangle elements. The axis of symmetry is on the left side of each figure. The models were computed with an explicit formulation with fixed time increments of 1 ns. The bulk element size in the plate was 1 mm and the bulk element size in the ball was 100 um. The mesh size was refined near the point of contact between the ball and plate, as shown in the figure. The smallest mesh size, which was at the location of contact, was 1 um.

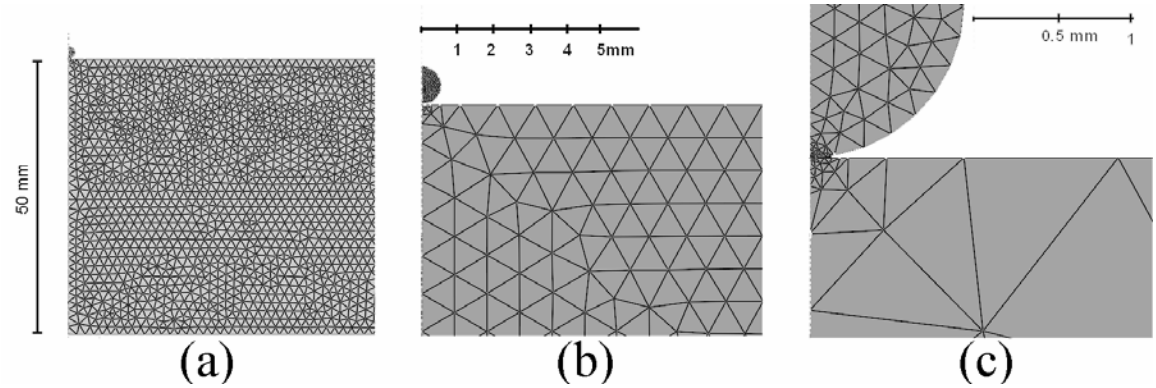

Figure 1. The axisymmetric finite element model of a 1.58 mm ball colliding with a massive plate at three different magnifications showing the mesh refinement near the point of contact.

The output from the finite element model is used as a quantitative check for both the solutions to the equations of elastodynamics and the Hertzian contact laws.

5. EXPERIMENTAL PROCEDURE

Figure 2 illustrates a typical experimental test arrangement. The arrow represents the location and direction of the source (in this case the impact of a ball). The test block used for these tests was either a massive mild steel plate

50mm thick and 600 mm square or a glass plate 24.4 mm thick and 76 mm square. At the maximum wave speed for steel (6000 m/s) it takes 100 μs for the stress waves to reach the edge of the plate and return to the center of the plate where the source and sensors are located. Therefore the first 100 μs of each sensor's record will be unpolluted by side reflections and the plate can be treated as infinite during this time period. A similar calculation on the glass plate gives 125 μs of unpolluted signal.

Sensors were located at three different orientations relative to the location of the ball drop. Location 1 is a surface location on the same side of the test block as the source. In this location most of the stress wave energy felt by the sensor is in the form of the Raleigh wave. Location 2 is the epicentral location. At this location all displacements are normal to surface of the plane of the plate and the stress wave energy is mainly in the form of the P wave. Location 3 is an off-epicentral location for which the particle displacements are at some oblique angle from the surface normal and a large portion of the stress wave energy arrives in the form of the S-wave. By comparing and contrasting the output from sensors at the three different locations the effects of the sensor aperture and directionality can be studied.

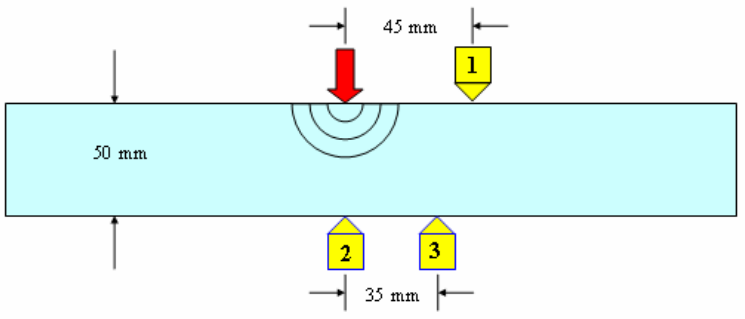

Figure 2. (color online) Experimental setup for ball drop tests.

The sensors used for these experiments were Glaser-NIST-type broad-band, piezoelectric displacement transducers[17], made in our laboratory, with initial design based on the NBS conical transducer[18]. The signals were recorded with a 14 bit High-Techniques™ digitizer at sampling rates of 5 MHz and 10 MHz.

6. RESULTS AND DISCUSSION

The sensor output from the collision of a 1.58 mm diameter hardened steel ball bearing dropped 31 mm onto the 50 mm thick steel plate is plotted in Figure 3 along with the surface displacements calculated from a finite element model and those calculated from the marriage of Hertz theory and the appropriate Green's function found from generalized ray theory. Figure 3 (a) shows the measured and calculated displacements at Location 2 (epicentral position), while Figure 3 (b) shows those at Location 3 (35mm off-epicenter). Figure 4 shows the sensor output, finite element results, and theoretical calculations at Location 2 due to the collision of a 0.79 mm ruby ball dropped 325 mm onto the glass plate.

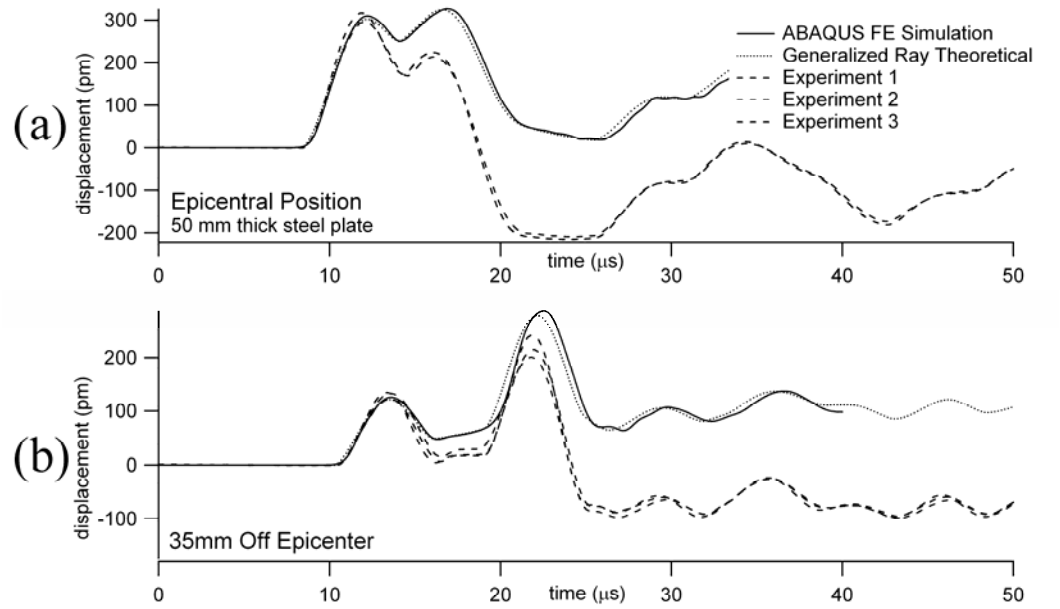

Figure 3. Comparison between calculated and measured displacements at Location 2 (a) and Location 3 (b) due to a 1.58 mm steel ball colliding with a massive steel plate.

These figure show that the displacements obtained from the finite element model very closely match the results from generalized ray theory. The experimental results are in good agreement with the two models at high frequencies, and the downward trend of the measured signals after contact initiation is due to the inability of the sensor to capture frequencies below approximately 8 kHz. The results of three different ball drops are shown in Figure 3 in order to emphasize the repeatability of the ball source. The displacements plotted in Figure 4 show similar results for the ruby ball on the glass plate. The frequency content of the displacements in this figure is somewhat higher than those in Figure 3, and it can be more easily seen that the displacements obtained from the finite element model deviate from theory at high frequencies. This can be seen most clearly at the onset of the arrival of the first waves.

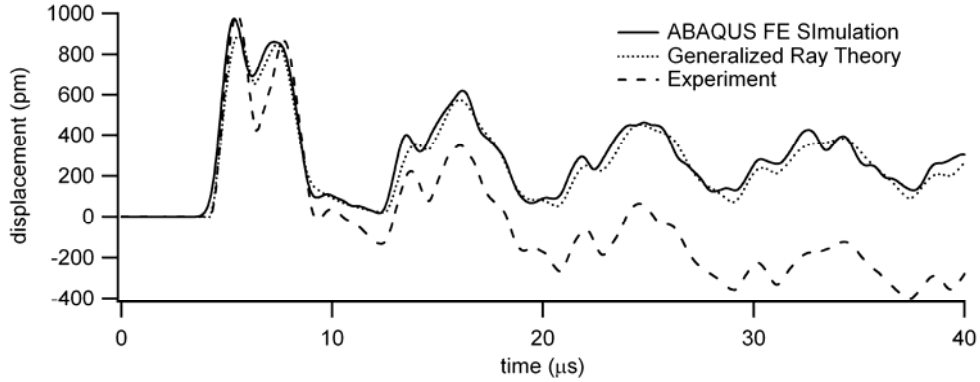

Figure 4. Comparison between calculated and measured displacements (at Location 2) due to a 0.79 mm ruby ball colliding with a massive glass plate.

The finite element model offers an excellent platform by which the elastic wave displacements can be visualized. Figure 5 shows the model of a 1.58 mm diameter steel ball colliding with a 50 mm thick steel plate (the same model whose displacements are plotted in Figure 3). The first row of figures (Figure 5 (a), (b), and (c)) show, at three different time frames, the displacements magnified by a factor of one thousand while the second row of figures (Figure 5 (d), (e), and (f)) show the same displacements, at the same time frames as the first row, magnified by a factor of ten million. The length scale of each row is shown on the left side of the figure and the time frames of each column are shown at the bottom of the figure.

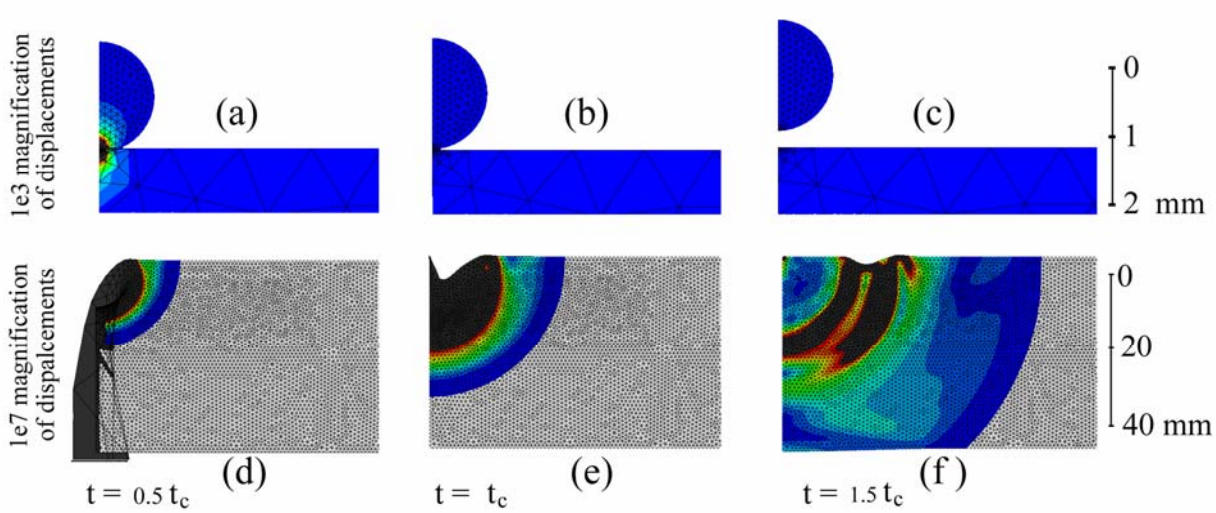

Figure 5 (color online). Displacements and stresses calculated from an axisymmetric finite element model of a 1.58 mm ball colliding with a massive plate at three different times and two different magnifications.

From this figure it can be seen that the deformations at the location of the impact between the ball and the plate are approximately four orders of magnitude larger than the displacements of the largest elastic waves which are radiated away from the location of contact. The largest amplitude elastic wave is the Rayleigh wave which propagates along the surface of the plate and is shown in Figure 5 (e) and (f).

Elastic Wave Energy

One parameter measured from elastic collisions which has been the subject of a significant amount of research over the last century is the coefficient of restitution, defined as the ratio of the magnitude of the incoming and rebound velocity of the ball[6,19]. If no energy is lost in the collision, the coefficient of restitution is unity. In real collisions some energy is always lost to inelasticity of the materials, such as plastic deformations and viscoelastic effects, and some energy is always lost to elastic waves which radiate away from the location of contact. It is desirable to know the exact quantity of energy radiated away in this manner, because this energy loss defines the upper bound on the coefficient of restitution which can be expected given perfectly elastic collisions[6,19].

In a finite element model, the displacements at every node are calculated at every time step, and from these displacements the velocities, accelerations, stresses, strains, and energy terms can be calculated. It is tempting to use the finite element model to estimate the amount of kinetic energy and strain energy carried in the propagating elastic waves, but this approach can yield very misleading results, as illustrated below.

Energy flux across a surface S which surrounds the source can be defined as the inner product of the elastic stress tensor with the particle velocity in the direction normal to the surface S. By substituting the appropriate equations for stress and strain to this equation, the energy flux is found to be linearly proportional to the square of the particle velocity normal to the surface S. By taking advantage of the derivative theorem of Fourier transforms[20]:

$$\mathrm{F}\left(\frac{du}{dt}\right) = iw\,\mathrm{F}(u) \tag{13}$$

where

$$\mathrm{F}(u) = \int_{-\infty}^{\infty} u e^{-iwt} dt \tag{14}$$

the energy flux across a point can be expressed as

$$E_{flux} \propto -\omega^2\,\mathrm{F}(u(t)^2) \tag{15}$$

where u(t) is the time history of displacements normal to the surface S described in Equation 12 and plotted in Figures 3 and 4.

The energy flux is presented in Figure 6 as a function of frequency for the displacement time histories shown in Figure 3(a), for arbitrary units. The figure shows that while most of the energy flux is found at frequencies less than 400 kHz, an appreciable fraction of the energy flux is contained at frequencies well into the MHz range. The finite element simulation deviates from theory at high frequencies (starting at about 700 kHz). This deviation at high frequencies occurs because the finite element model cannot accurately capture the high-frequency short-wavelength elastic waves when the wavelength becomes so small that it approaches the size of the elements in the model.

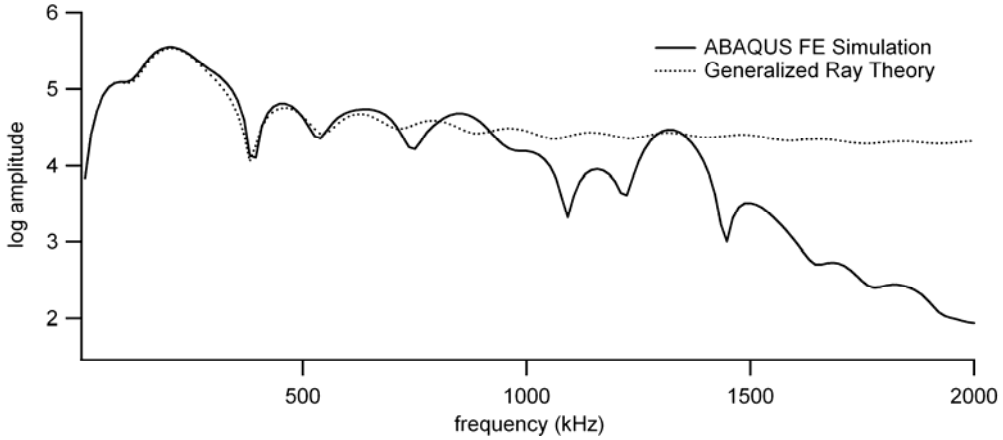

Figure 6. Energy as a function of frequency contained in the stress waves radiated from the impact of a 1.58 mm steel ball on a massive steel plate.

For the collision between the 1.58 mm steel ball and a steel plate described above and shown in Figures 3, 5, and 6 (t_c= 5.5 us), only about eight percent of the total energy flux at the epicentral location is above 700 kHz, but for the collision between the 0.79 mm ruby ball and glass plate (t_c= 2.2 us), shown in Figure 4, about forty-six percent of the energy flux at this location is above 700 kHz. The difficulty in estimating elastic wave energy from a finite element model is that the frequency at which the model deviates from reality is dependent upon the characteristics of the finite element model while the percent of the total energy flux which is above this frequency is dependent on the characteristics of the ball source and the angle of incidence of the ray path between the source and the sensor.

7. CONCLUSIONS

The collision of a tiny ball and a massive plate and the elastic waves produced from this source have been described theoretically, modeled numerically, and measured experimentally. A marriage of the Hertz theory of contact and a generalized ray theoretical solution to the full elastodynamic equations of motion in an elastic body were utilized to find displacement time histories of the plate's surface as a function of ball geometry, approach velocity, and material properties. These displacements were then compared to those measured by Glaser-NIST conical piezoelectric sensors and those calculated by the finite element program ABAQUS. The good agreement between the theoretical, numerical, and experimental results demonstrates that both the sensors and the finite element model can be calibrated via this method. It was also shown that the sensor response deviates from theory at low frequencies and the finite element model fails to capture the elastic wave displacement at high frequencies, where the wavelengths become so small that they approach the element size in the finite element model.

On first inspection, it may appear possible to estimate the total energy in the propagating elastic waves via the calibrated finite element model, but a significant fraction of the elastic wave energy is carried at frequencies well into the MHz range which the model fails to capture. This study shows that extreme caution is warranted when interpreting the results of finite element models, even when they appear to be calibrated.

8. AKNOWLEDGEMENTS

This work was funded by NSF-GRF and NSF grant CMS-0624985.

9. REFERENCES

[1] Breckenridge, F., Tscheigg, C., and Greenspan, M., "Acoustic emission: some applications of Lamb's Problem", Journal of the Acoustical Society of America, 57(3), pp. 626-631, (1975).

[2] Breckenridge, F., Proctor, T., Hsu, N., Fick, S., Eitzen, D., "Transient Sources for Acoustic Emission Work," in Progress in Acoustic Emission V, Yamaguchi, K., Takahashi, H., and Niitsuma, H., The Japanese Society for NDI, Sendai, Japan, pp. 20-37, (1990).

[3] Love, A.E. H., [A treatise on the mathematical theory of elasticity], Cambridge Univeristy Press London, Chapter 8 (1934).

[4] Johnson, K. [Contact Mechanics], Cambridge University Press, Cambridge, Chapter 11, (1985).

[5] Goldsmith, W., [Impact], Dover Publications, New York, Chapters 1 and 4, (2001).

[6] Hunter, S. C., "Energy absorbed by elastic waves during impact," Journal of the Mechanics and Physics of Solids, 5, pp.162-171, (1957).

[7] Lamb, H., "On the Propagation of Tremors over the Surface of an Elastic Solid," Philosophical Transactions of the Royal Society of London A 203, pp. 1-42, (1904).

[8] Miller, G. F. and Pursey, H., "The field and radiation impedence of mechanical radiators on the free surface of a semi-infinite isotropic solid," Proc. Royals Society of London. Series A, 223, pp. 521-541, (1954).

[9] Pekeris, C. L., "The Seismic Surface Pulse," Proceedings of the National Academy of Sciences 41,pp. 469-480, (1955).

[10] Knopoff, L. "Surface motions of a thick plate," Journal of Applied Physics, 29(4), pp. 661-670 (1958).

[11] Johnson, L., "Green's Function for Lamb's Problem," Geophys. J. R. astro. Soc. 37, pp.99-131, (1974).

[12] Aki, K., Richards, P. G., [Quantitative Seismology: Theory and Methods], Freeman, San Francisco, Chapter 4, (1980).

[13] Graff, K, [Wave Motion in Elastic Solids], Oxford University Press, Mineola, NY, Chapters 5 and 6, (1975).

[14] Helmberger, D. "Generalized ray theory for shear dislocations," Bulletin of the Seismological Society of America, 64(1) pp.45-64, (1974).

[15] Ceranoglu, A., and Pao, Y. "Propagation of elastic pulses and acoustic emission in a plate," Journal of Applied Mechanics: Transactions of the ASME 48, pp. 125-147, (1981).

[16] ABAQUS, Version 6.7-1, Hibbitt. Pawtucket, RI, Karlsson & Sorensen, 2006.

[17] Glaser, S., Weiss, G., and Johnson, L., "Body Waves Recorded Inside an Elastic Half-space by an Embedded, Wideband Velocity Sensor," Journal of Acoustic Society of America, 104, pp. 1404-1412, (1998).

[18] Proctor, T. M. "An improved piezoelectric acoustic emission transducer," Journal of Acoustic Society of America, 71, pp.1163-1168, (1982).

[19] Reed, J. "Energy losses due to elastic wave propagation during an elastic impact," Journal of Physics D: Applied Physics, 18, pp. 2329-2337, (1985).

[20] Bracewell, R. [The Fourier transform and its applications], McGraw-Hill, Boston, Chapter 6, (2000).